REPORT DOCUMENTATION PAGE

Form Approved OMB NO. 0704-0188

1. REPORT DATE (DD-MM-YYYY)	2. REPORT TYPE	3. DATES COVERED (From - To)
07-01-2019	Final Report	5-Sep-2011 - 4-Sep-2017

4. TITLE AND SUBTITLE
Final Report: Anode and Electrolyte Chemistries for Mg-Based Secondary Batteries

5a. CONTRACT NUMBER
W911NF-11-1-0432

5b. GRANT NUMBER

5c. PROGRAM ELEMENT NUMBER
611102

6. AUTHORS

5d. PROJECT NUMBER

5e. TASK NUMBER

5f. WORK UNIT NUMBER

7. PERFORMING ORGANIZATION NAMES AND ADDRESSES
Arizona State University
ORSPA
P.O. Box 876011
Tempe, AZ 85287 -6011

8. PERFORMING ORGANIZATION REPORT NUMBER

9. SPONSORING/MONITORING AGENCY NAME(S) AND ADDRESS (ES)
U.S. Army Research Office
P.O. Box 12211
Research Triangle Park, NC 27709-2211

10. SPONSOR/MONITOR'S ACRONYM(S)
ARO

11. SPONSOR/MONITOR'S REPORT NUMBER(S)
58832-CH.5

12. DISTRIBUTION AVAILIBILITY STATEMENT
Approved for public release; distribution is unlimited.

13. SUPPLEMENTARY NOTES
The views, opinions and/or findings contained in this report are those of the author(s) and should not contrued as an official Department of the Army position, policy or decision, unless so designated by other documentation.

14. ABSTRACT

15. SUBJECT TERMS

16. SECURITY CLASSIFICATION OF:			17. LIMITATION OF ABSTRACT	15. NUMBER OF PAGES	19a. NAME OF RESPONSIBLE PERSON
a. REPORT	b. ABSTRACT	c. THIS PAGE			Daniel Buttry
UU	UU	UU	UU		19b. TELEPHONE NUMBER 480-965-2476

RPPR Final Report
as of 14-Jan-2019

Agency Code:

Proposal Number: 58832CH **Agreement Number: W911NF-11-1-0432**
INVESTIGATOR(S):

Name: PhD Daniel A. Buttry
Email: dbuttry@asu.edu
Phone Number: 4809652476
Principal: Y

Organization: **Arizona State University**
Address: ORSPA, Tempe, AZ 852876011
Country: USA
DUNS Number: 943360412 EIN: 860196696
Report Date: 04-Dec-2017 Date Received: 07-Jan-2019
Final Report for Period Beginning 05-Sep-2011 and Ending 04-Sep-2017
Title: Anode and Electrolyte Chemistries for Mg-Based Secondary Batteries
Begin Performance Period: 05-Sep-2011 **End Performance Period:** 04-Sep-2017
Report Term: 0-Other
Submitted By: PhD Daniel Buttry Email: dbuttry@asu.edu
Phone: (480) 965-2476
Distribution Statement: 1-Approved for public release; distribution is unlimited.

STEM Degrees: 6 **STEM Participants:** 8

Major Goals: The specific project goals were:
(a) Use of spectroscopic methods to understand the solvation environment for Mg2+ in ionic liquid electrolyte systems.
(b) Correlate the spectroscopic measurements with electrochemical investigative results of the Mg/Mg2+ redox couple.
(c) Gain insight into the varying electrochemical mechanisms for the deposition and dissolution processes
(d) Identify the electroactive species for successful Mg electrodeposition.

The overarching project goals were to learn to control the coordination environment of Mg2+ in ionic liquids electrolytes so as to achieve reversible electrodeposition and electrodissolution of the Mg2+/Mg redox couple to enable magnesium batteries based on Mg metal anodes.

Accomplishments: see attached pdf

Training Opportunities: A number of different graduate made a variety of contributions to the effort during the course of the grant. The list is given in the Participants section. In most cases, these were relatively minor contributions. In a few cases, these contributions were significant. Tylan Watkins did the bulk of the work on the grant. He was supported a total of 42 months on the grant (note the field available to indicate duration of support in the Participants section did not allow me to enter the proper number). Jarred Olson was an undergraduate student who did a lot of the early work in ionic liquids in our group. He was supported a total of 7 months. Ashok Kumar (9 months) made some key measurements that helped confirm our hypotheses of how BH4- and free glymes influenced the Mg2+/Mg redox chemistry. Joe Rheinhardt (13 months) picked up the project after Tylan graduated. He helped finish off the project and has driven the transition to our new effort in calcium anode chemistry.

Results Dissemination: see attached pdf

Honors and Awards: Nothing to Report

Protocol Activity Status:

Technology Transfer: Nothing to Report

RPPR Final Report
as of 14-Jan-2019

PARTICIPANTS:

Participant Type: PD/PI
Participant: Daniel Alan Buttry
Person Months Worked: 2.00 **Funding Support:**
Project Contribution:
International Collaboration:
International Travel:
National Academy Member: N
Other Collaborators:

Participant Type: Graduate Student (research assistant)
Participant: Tylan Strike Watkins
Person Months Worked: 15.00 **Funding Support:**
Project Contribution:
International Collaboration:
International Travel:
National Academy Member: N
Other Collaborators:

Participant Type: Graduate Student (research assistant)
Participant: Ashok Kumar
Person Months Worked: 9.00 **Funding Support:**
Project Contribution:
International Collaboration:
International Travel:
National Academy Member: N
Other Collaborators:

Participant Type: Graduate Student (research assistant)
Participant: Daniel Mahlman
Person Months Worked: 7.00 **Funding Support:**
Project Contribution:
International Collaboration:
International Travel:
National Academy Member: N
Other Collaborators:

Participant Type: Graduate Student (research assistant)
Participant: Rajeev Ranjan
Person Months Worked: 2.00 **Funding Support:**
Project Contribution:
International Collaboration:
International Travel:
National Academy Member: N
Other Collaborators:

Participant Type: Undergraduate Student
Participant: Jarred Olson
Person Months Worked: 7.00 **Funding Support:**
Project Contribution:
International Collaboration:
International Travel:
National Academy Member: N

Other Collaborators:

Participant Type: Graduate Student (research assistant)
Participant: Joseph Rhenihardt
Person Months Worked: 13.00 **Funding Support:**
Project Contribution:
International Collaboration:
International Travel:
National Academy Member: N
Other Collaborators:

Participant Type: Graduate Student (research assistant)
Participant: Christopher Starr
Person Months Worked: 4.00 **Funding Support:**
Project Contribution:
International Collaboration:
International Travel:
National Academy Member: N
Other Collaborators:

Participant Type: Graduate Student (research assistant)
Participant: James Thorne
Person Months Worked: 2.00 **Funding Support:**
Project Contribution:
International Collaboration:
International Travel:
National Academy Member: N
Other Collaborators:

ARTICLES:

Publication Type: Journal Article Peer Reviewed: Y **Publication Status:** 1-Published
Journal: Journal of the American Chemical Society
Publication Identifier Type: DOI Publication Identifier: 10.1021/jacs.5b11031
Volume: 138 Issue: 2 First Page #: 641
Date Submitted: Date Published: 1/1/16 12:00AM
Publication Location:
Article Title: Designer Ionic Liquids for Reversible Electrochemical Deposition/Dissolution of Magnesium
Authors: Tylan Watkins, Ashok Kumar, Daniel A. Buttry
Keywords: magnesium battery ionic liquid
Abstract: Chelating ionic liquids (ILs), in which polyether chains are pendent from the organic pyrrolidinium cation of the ILs (PEGylated ILs), were prepared that facilitate reversible electrochemical deposition/dissolution of Mg from a Mg(BH4)(2) source. Mg electrodeposition processes in two specific PEGylated-ILs were compared against that in the widely studied N-butyl-N-methylpyrrolidinium bis(trifluoromethylsulfonyl)imide ionic liquid (BMPyrTFSI). Reversible Mg electrodeposition was achieved with high Coulombic efficiency (CE) of 90% and high current density (ca. 2 mA/cm(2) for the stripping peak). Comparison of the different IL electrolytes suggested that these displacement reactions may play a role in enabling Mg deposition/dissolution with high CE and current density in these PEGylated IL media. These results represent the first demonstration of reversible electrochemical deposition/dissolution of Mg in an ionic liquid specifically designed with this task in mind.
Distribution Statement: 1-Approved for public release; distribution is unlimited.
Acknowledged Federal Support:

RPPR Final Report
as of 14-Jan-2019

Final Report

AMSRD-ARL-RO-SI Proposal Number: 58832-CH

Agreement Number: W911NF-11-1-0432

Reporting Period: September 5, 2011 to September 4, 2017

Daniel A. Buttry

School of Molecular Sciences, Arizona State University

PO Box 871604 Tempe, AZ 85287-1604

Anode and Electrolyte Chemistries for Mg-Based Secondary Batteries

Abstract

We describe the results of a multiyear study designed to understand how the coordination environment for Mg^{2+} in ionic liquids influences its electrochemical behavior, with an emphasis on the development of conditions that enable reversible Mg electrodeposition. We describe below a sequence of experimental studies that revealed a pathway to reversible electrodeposition. Ultimately, we were successful in showing that control of two factors could enable reversible electrodeposition. These two factors were: 1) limiting trace water content in the electrolyte, and 2) prevention of $TFSI^-$ coordination at the Mg^{2+} metal center. Using a novel synthetic strategy, we were able to demonstrate the highest coulombic efficiency ever reported for Mg^{2+}/Mg redox in an ionic liquid.

Report

The overall project goals remained essentially the same throughout the entire project period and were:

(a) Use of spectroscopic methods (especially Raman) to understand the solvation environment for Mg^{2+} in IL electrolyte systems.
(b) To correlate the spectroscopic measurements with electrochemical investigative results of the Mg/Mg^{2+} redox couple.
(c) Gain insight into the varying electrochemical mechanisms for the deposition and dissolution processes
(d) Identify the electroactive species for successful Mg electrodeposition.

Due to the theoretical metrics of a rechargeable battery using a magnesium anode (notably 3832 mAh/cm^3 volumetric and 2205 mAh/g gravimetric capacities) there have been significant efforts to develop electrolytes and cathode materials for secondary Mg batteries. From the perspective of the DOD, the earth abundance of Mg gives it a special advantage in comparison to other battery materials with lower abundance and/or access that could be limited by geopolitical issues, such as Li. Thus, magnesium batteries have a special attraction to DOD.

Our efforts in this area started with preliminary studies designed to understand the factors that limited reversible electrodeposition for Mg metal in IL's. Thus, we focused on obtaining high

Figure 1. Picture of electrochemical cell set-up attached to the vacuum line. The cell consists of four necks, one for each electrode and one for connecting the cell to the vacuum line. Wires connecting the electrodes to the external circuit are sealed with leaded glass.

quality electrochemistry of Mg/Mg^{2+} in various ionic liquids. This involved determining the sensitivity of the electrochemistry to impurities and other influences of the medium. To summarize the results before presenting the details, we offer the key finding which is that water content is a CRITICAL element in determining whether or not high quality electrochemistry will be obtained for the Mg/Mg^{2+} redox couple in ILs. Specifically, when water is present even at very low concentrations, we observe very poor (chemical) reversibility of the electrochemical deposition and stripping. We determined this is due to surface passivation driven by reaction of Mg metal with water, generating an insulating MgO or $Mg(OH)_2$ film. Thus, we focused on identifying experimental conditions in which we could produce extremely dry ILs and then examined Mg electrochemistry. We devoted considerable time and energy to obtaining dry ILs and characterizing the water content. This involved designing an experimental system allowing us to do electrochemistry on a high vacuum line (shown in Figure 1). We also designed and built a first prototype of a thin layer cell (shown in Figure 2) whose function is to allow us to use a "getter" electrode to scavenge water from the electrolyte so we can produce highly pure conditions. We describe results below based on these experimental conditions. As described, after this part of the effort we focused on two key tasks. (1) Using the ultrapure ILs we learned to prepare, we started using various spectroscopic methods to characterize the complexation around Mg^{2+} in the ILs. (2) Using these ultrapure ILs, we initiated a study of the deposition of Mg and its electrochemical reversibility.

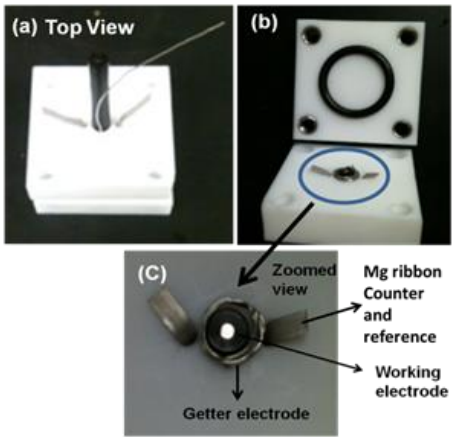

Figure 2. Pictures of thin electrochemical cell design showing the top view in (a), inner view in (b) and the zoomed view of getter, working, counter and reference electrodes in (c).

Preliminary experiments, results and discussion

The preliminary experiments were performed to examine the electrochemistry of Mg/Mg^{2+} in IL system using cyclic voltammetry (CV) techniques. The results are as follows. The reversible deposition-dissolution behavior of Mg in $Mg(ClO_4)_2/Pyr_{14}TFSI$ in comparison to $Pyr_{14}TFSI$ is shown in Figure 3. Compared to the background (red curve, $Pyr_{14}TFSI$), the black curve ($Mg(ClO_4)_2/Pyr_{14}TFSI$) shows a cathodic wave at +0.87 V and +0.21 V. (Note that the potential of the reference here is not the true Mg/Mg^{2+} potential due to adsorption effects we are still exploring.) We believe the second (more negative) peak corresponds to Mg deposition. The anodic peak observed at +1.64 V is clearly associated with magnesium dissolution in solution as it is obtained using $Mg(ClO_4)_2$ and is never observed while scanning the IL by itself. Furthermore, the shape of the anodic wave is highly indicative of a metal stripping peak as opposed to a diffusion limited process. This peak current also increases with Mg concentration (see below). The cathodic peak around +0.16 V in control experiment is likely associated with an impurity inherently found in the IL itself and could be additive in the bulk Mg deposition occurring at the same potential.

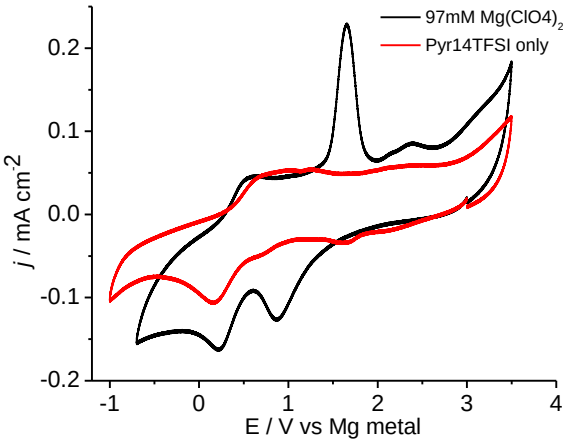

Figure 3. Cyclic voltammogram comparing Mg deposition and re-dissolution from 97 mM $Mg(ClO_4)_2$ in $Pyr_{14}TFSI$ (black curve) with $Pyr_{14}TFSI$ by itself (red curve) as a control, scan rate: 0.2 V/s.

Figure 4 shows a series of voltammograms taken at various cathodic potential limits. Cycle 1 shows almost no evidence of Mg deposition and dissolution in $Mg(ClO_4)_2Pyr_{14}TFSI$. The bulk reduction of Mg does not occur until the potential of the negative limit is less than approximately 0 V vs a Mg reference. Then, a clear increase of Mg deposition and dissolution is observed after scanning to more negative potentials (from cycle 2 to cycle 4). Hence, the reduction peak around 0.3V to 0.4V is attributed to Mg^{2+}/Mg, and the oxidation peak around +1.87 V is the stripping peak of electrodeposited Mg.

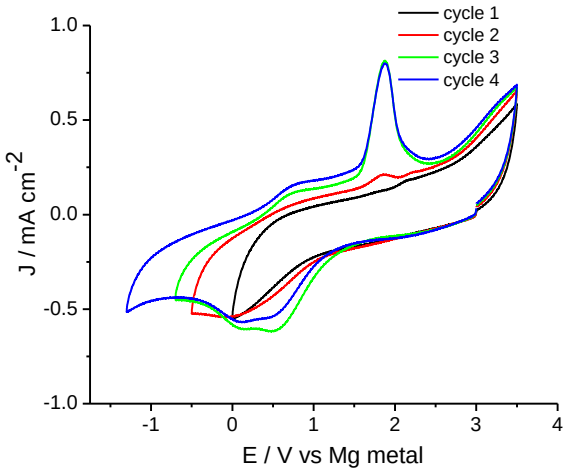

Figure 4. Cyclic voltammogram of Mg deposition-dissolution from 97 mM $Mg(ClO_4)_2Pyr_{14}TFSI$ on Pt disk electrode with an increase in negative potentials from cycle 1 to cycle 4, scan rate: 0.2 V/s.

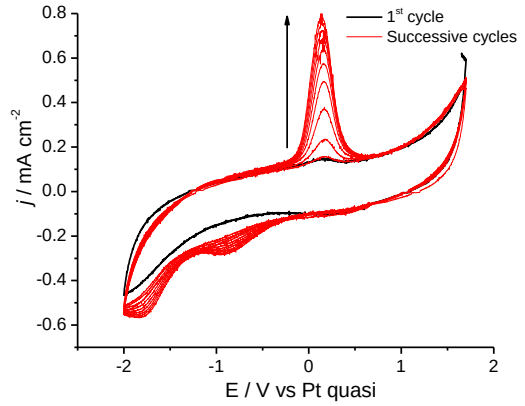

Figure 5. Cyclic voltammogram showing successive cylces of Mg deposition-dissolution from 149 mM $Mg(ClO_4)_2Pyr_{14}TFSI$ on Pt disk electrode, scan rate: 1V/s.

In a similar experiment, we also examined the effect of successive cycles over a constant potential range on the behavior of Mg deposition/dissolution (shown in Figure 5). A clear buildup of the anodic as well as cathodic peaks is noticed upon successive cycles. However, the reversible deposition-dissolution of Mg is not observed in the first cycle, which probably relates with the presence of water in IL. We believe this may be due to formation of a passive film of MgO or $Mg(OH)_2$ caused by the presence of water. Despite long drying times (≥24hrs) at 130°C and 10^{-5}Torr we feel these data suggest a passivation layer(s) is caused by the presence of trace water, hindering the deposition and/or stripping of Mg until sufficient cycling has caused the consumption of most water within the diffusion layer. Thus, the chemical reversibility for redox chemistry of Mg is improved as we consume water in near surface region by cycling.

These findings prompted us to design a "thin cell" (shown in Figure 2) in order to bypass the problem with trace amounts of water. The basic idea of the cell is to have as little volume of solution around the working electrode as possible. This should allow all water within a region to diffuse to the electrode and to be completely consumed by cycling a "getter" electrode prior to electrochemical measurements on working electrode. The present cell design is similar to how Li batteries are designed using a very thin electrolyte and a large electrode.

We also explored the dependence of the Mg stripping peak on the concentration of Mg^{2+} in the solution. This comparison is shown in Figure 6. A clear increase in the deposition/stripping peak is observed on going from 100 mM $Mg(TFSI)_2$ to 300 mM $Mg(TFSI)_2$. This strongly supports our assignment of this peak as a Mg stripping peak and proves the contribution of Mg for cathodic and anodic peaks.

The net result of these early studies showed the importance of trace levels of water in the

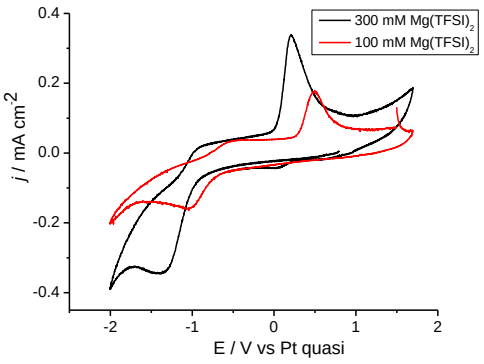

Figure 6. Comparison of Mg deposition-dissolution with different concentrations of $Mg(TFSI)_2$ in $Pyr_{14}TFSI$ on Pt disk electrode, scan rate: 0.2 V/s.

electrolyte. This ultimately drove us to design electrolyte systems containing borohydride anion, which is reactive with water. We will describe this part of the effort further below.

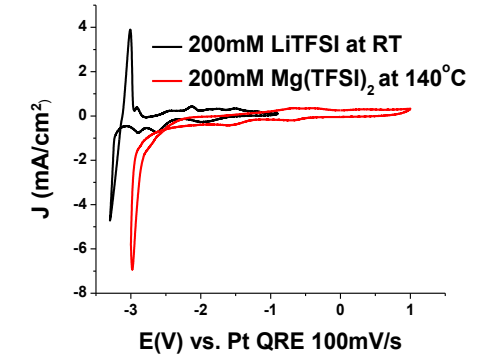

a)

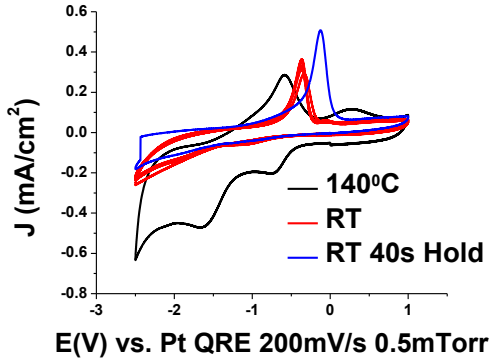

b)

Figure 7: a) Comparison of $Mg(TFSI)_2$/BMPTFSI at 140°C to LiTFSI/BMPTFSI at RT.
b) Comparison of Mg UPD on Pt at RT and 140°C. Blue scan was held at -2.5V for 40s at RT

The impact of coordination of Mg^{2+}

In the first reporting period we developed experimental techniques used in an effort to remove and avoid water in the solutions under study. While high vacuum techniques have certainly accomplished this aim, and have improved the ability to reproduce experimental outcomes, we found that it is not simply just a matter of establishing extremely dry conditions. Figure 7a demonstrates cyclic voltammograms acquired under high vacuum at 140°C in the case of $Mg(TFSI)_2$/BMPTFSI and room temperature in a glove box filled with nitrogen (2.5ppm H_2O, 1.5ppm O_2) for LiTFSI/BMPTFSI, after drying the solution for over 9 hours prior to the experiment. The 140°C scans were taken prior to the room temperature scans. Significant current at -2.8V vs a Pt quasi reference electrode (QRE) is attributed to bulk Mg deposition. This is compared to the Li/Li^+ redox system in the same IL using the LiTFSI salt; a scan acquired at room temperature. The approximately 700mV difference between the Mg^{2+}/Mg current and the Li^+/Li current is appropriate for the two couples in terms of expected thermodynamic behavior ($E°Mg/Mg^{2+}$ = -2.37V, $E°Li/Li^+$ = -3.05V vs SHE). In 7b under potential depositions are shown in which Mg was deposited on Pt at a potential approximately 1V more positive to that of Mg bulk deposition, shown in 7a. This potential difference is consistent with the difference in the work function of the two metals. At the higher temperature the cathodic current was greater and the process was slightly more reversible. The significant finding here was that bulk deposition of magnesium in this system leads to surface passivation which prevents reversibility. This occurs even in the driest conditions obtainable and suggested water is not the factor limiting the desired electrical response here.

To achieve a deeper understanding of the complexities of the situation we used Raman spectroscopy to probe the nature of the Mg^{2+} solvation/coordination environment. Analogous Li^+ solvation in $TFSI^-$ based ILs has been reported on by several authors who have found that Li^+ exists in an environment in which it is speciated as $Li[TFSI]_2^-$. We found a similar situation for Mg^{2+}, in that it exists as the anion $Mg[TFSI]_3^-$. This is an unwanted complexation because it will ultimately hinder the Mg^{2+} transference number. In other words, the anionic speciation of Mg^{2+} acts against its delivery to the anode during electrodeposition, thus inhibiting the overall electrochemical process. Figure 8 shows Raman data taken for $Mg(TFSI)_2$/BMPTFSI solutions as

well as other dissolved Mg^{2+} salts in the same IL. $Mg(TFSI)_2$ showed the greatest miscibility, being soluble up to a 50% molar ratio with respect to BMPTFSI. Figure 8a shows the Raman spectrum for BMPTFSI from 87-2000cm^{-1}. The inset displays the ~742cm^{-1} peak which has been attributed to "free" $TFSI^-$ anions ($TFSI^-$ anions not coordinating with the metal cation) Figure 8b shows the raw data being fit by two Voigt curves fixed at 40% Gaussian and 60% Lorentzian with line widths between 9 and 11 for the 742 peak and 8-9 for the 752 peak. These Voigt profiles resulted in the best overall fit of the data, are consistent with profiles used in LiTFSI studies, and are justifiable due to the highly viscous nature of the liquids. The areas under the fitted curves were used to quantify relative polulations of TFSI states. Figure 8c displays the fraction of coordinated $TFSI^-$ anions as a function of the $Mg(TFSI)_2$ molar concentration, using $[Mg(TFSI)_2]_x[BMPTFSI]_{1-x}$ to express the material composition (a common notation throughout the LiTFSI literature and thus used here for comparison). It is clear from this plot that TFSI coordinates with Mg^{2+} as a *tris* complex. Plotted alongside the $Mg(TFSI)_2$ data points in 8d are those for other MgX_2 salts (X=$ClO4^-$, I^-,Br^-, Cl^-). The magnesium halides were only soluble up to about 200mM (x=0.054) at room temperature. Samples above this concentration were heated to about 40°C to maintain a liquid state. $MgCl_2$ and $MgBr_2$ do not show an increased Mg-TFSI peak above x=0.054 as clearly observed in the plot. MgI_2 does, however, show an increase in the coordinated peak when the sample was heated. It is unclear if this was due to an increased solubility at higher temperatures or a difficulty with the measurement as MgI_2 solutions at higher concentrations gave drastically greater fluorescence in the background (solution was yellow/orange in color). $Mg(ClO_4)_2$ was much more soluble but not as soluble as $Mg(TFSI)_2$ as it maxed out at 1.5M (x=0.3).

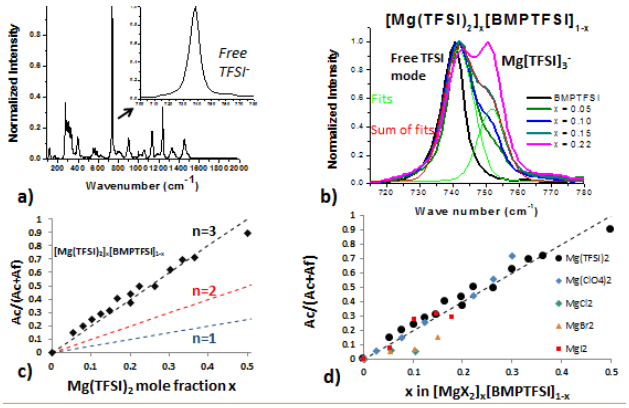

Figure 8: a) BMPTFSI Raman spectrum from 87-2000cm-1. Inset displays 742cm-1 free TFSI peak at 742cm-1. b) Spectra acquired over range of concentrations for Mg(TFSI)2/BMPTFSI with Voigt curve fits. C) Measured fraction Mg-TFSI/total TFSI. D) Mg(TFSI)2 compared to other MgX2 salts. Error bars fit within symbols.

Also noted with LiTFSI studies is that a change in the IL cation has a negligible effect on the $TFSI^-$ coordination with Li^+. We found this to also hold true for Mg^{2+}. The coordination of the metal with $TFSI^-$ can be varied drastically, however, by adding species with a known affinity for the metal cation centers. Glymes have been known to coordinate well with Li+ for some time and have been extensively studied for their use in several electrolyte systems. Figure 9 shows a Raman analysis of complexation in solutions containing glymes. We were interested in improving the Mg^{2+} coordination in a similar manner, for the purpose of producing solutions capable of undergoing rapid, reversible Mg electro-deposition and dissolution. So, we next turned to investigations using glymes with the Mg^{2+}/BMPTFSI solutions.

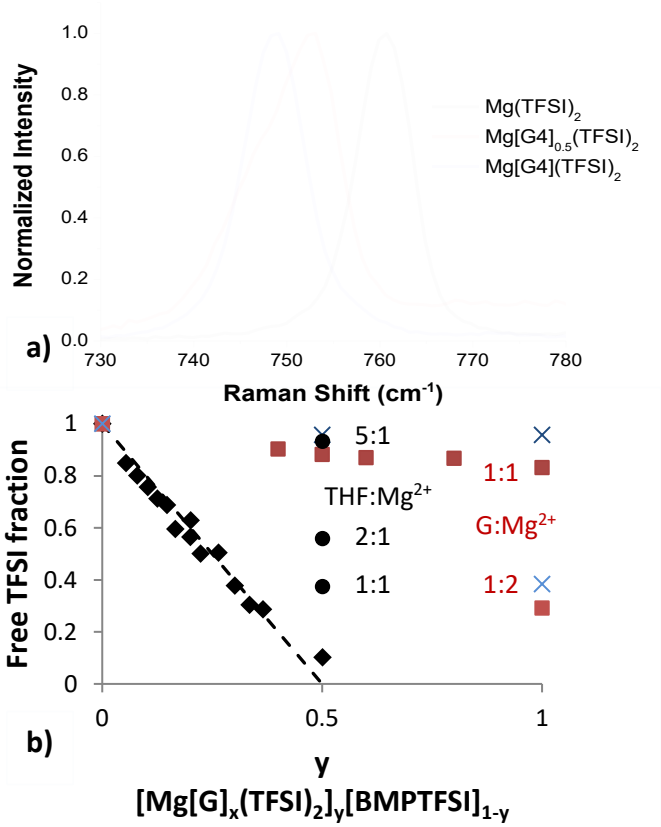

Figure 9: a) Raman of $Mg(TFSI)_2$ plotted alongside $Mg[G4]_{0.5}(TFSI)_2$ and $Mg[G4](TFSI)_2$. b) Fraction of Free $TFSI^-$ as a function of $Mg(TFSI)_2$ molar concentration (black diamonds); dashed line represents trend for n=3. Also plotted are solutions prepared with known $THF:Mg^{2+}$ ratios (black circles) and $G:Mg^{2+}$ ratios (red squares G3, blue Xs G4). G2 was also used and found to give values equivalent to G3.

Speciation of Mg^{2+} in the BMPPyrTFSI Ionic Liquid

Raman spectroscopy on a series of $Mg(TFSI)_2$ and BMPyrTFSI solutions (denoted by the formula $[Mg(TFSI)_2]_x[BMPyrTFSI]_{1-x}$) revealed interesting trends in the solvation of Mg^{2+} by $TFSI^-$ anions. Figure 10a demonstrates how an increase in the $Mg(TFSI)_2$ concentration led to an increase in the band centered at $752cm^{-1}$. This band is attributed to $TFSI^-$ in a bidentate coordination with Mg^{2+}. Deconvolution of the peaks in this region with three Pseudo-Voigt functions, as depicted in figure 11, led to a quantitative assessment of the various $TFSI^-$ populations; namely, free, monodentate and bidentate coordinated anions. Figure 12 shows how this quantitative evaluation gave rise to a trend in which the solvation number (total $TFSI^-$ surrounding each Mg^{2+}) decreases as the concentration of $Mg(TFSI)_2$ increases, eventually leveling off around 3. In figure 10b a region of the spectra is shown that gives information on geometrical arrangement of the free and coordinated $TFSI^-$ anions. It was found that coordinated $TFSI^-$ anions prefer a cis geometry despite it being the higher energy isomer.

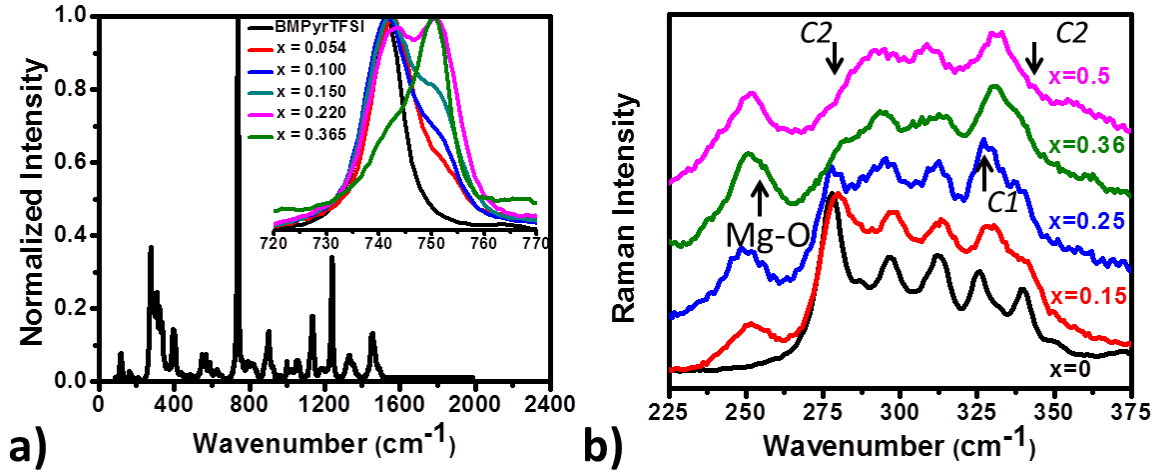

Figure 10: a) BMPyrTFSI Raman spectrum from 87-2000cm^{-1}. Inset displays 720cm^{-1} to 770cm^{-1} region at varying compositions. b) Spectra in the 225cm^{-1} to 375cm^{-1} region. Spectral intensities are shifted for clarity. C1 and C2 highlight the bands belonging to cis and trans conformers respectively.

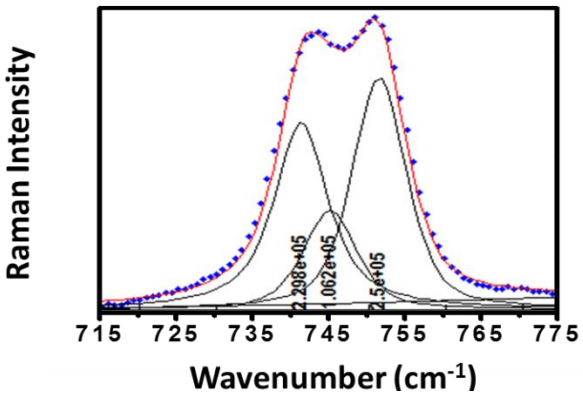

Figure 11: Pseudo-Voigt function fits of the raw Raman data between 715cm^{-1} and 775cm^{-1}. Numbers under the curves depict the respective intensities of each peak

Figure 13 shows the trend for each of the fit peaks; the 742cm^{-1}, 746cm^{-1}, and 752cm^{-1} peaks being the free, monodentate, and bidentate coordinated anions, respectively. At higher concentrations TFSI$^-$ prefers a bidentate coordination geometry, likely due to an entropic advantage as more anions remain uncoordinated when those that are coordinated maintain a maximum number of oxygens linked with a given Mg^{2+}. Finally, figure 14a demonstrates that addition of chelating agents, triglyme (G3) in this case, leads to a decrease in the number of coordinated TFSI$^-$. Figure 14d depicts the trends followed by each chelator studied. Each chelator fully removes TFSI^{-1} coordination when 6 ether oxygens are available per Mg^{2+} ion. In 14b it is clear that ether oxygens are coordinating Mg^{2+}

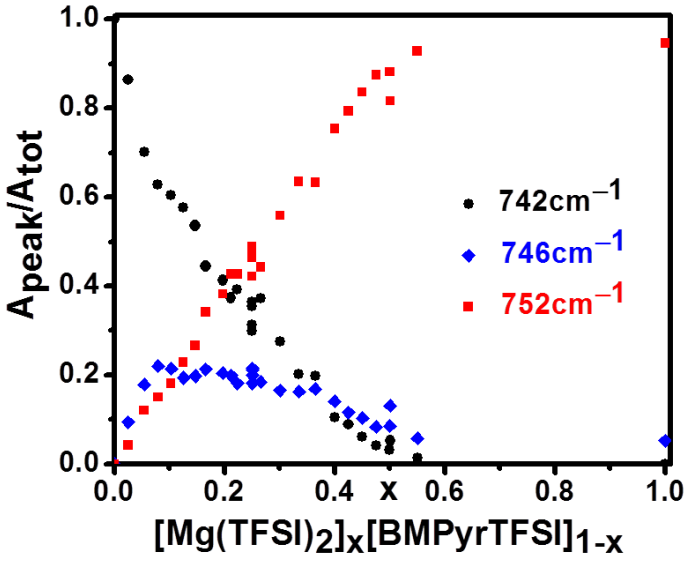

Figure 13: Fractional area of each of the three fit peaks.

of the chelating agents.

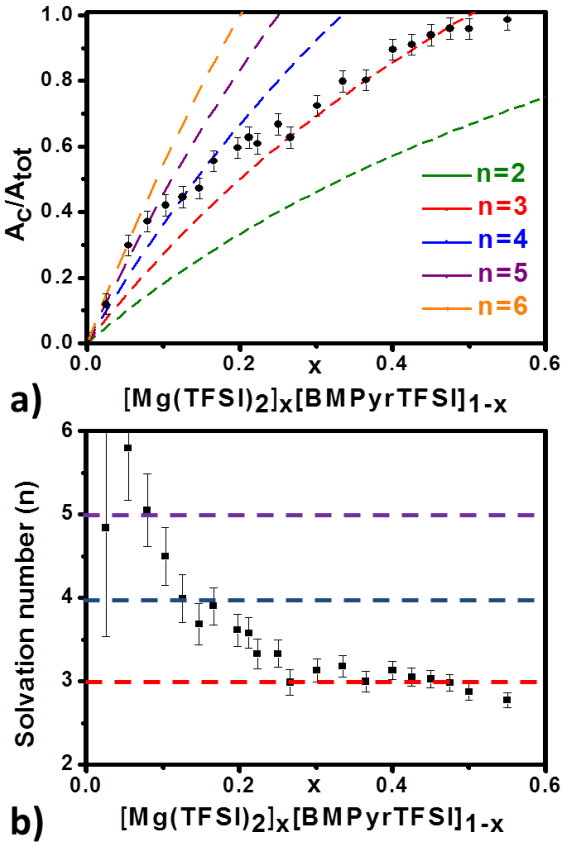

Figure 12: a) Fraction of TFSI$^-$ coordinated to Mg^{2+} with respect to the mole fraction of $Mg(TFSI)_2$ in the solution. Dashed curves follow theoretical trends for given solvation numbers. b) Calculated solvation numbers as a function of x.

as they give rise to a peak centered at 880cm^{-1} while free ethers give a broad set of bands from 780cm^{-1} to 860cm^{-1}. Similar to figure 13, figure 14c shows the changes in the TFSI^{-1} coordinated states as a function of the G3/Mg^{2+} ratio. Here, more G3, leads to more monodentate coordintation from TFSI^{-1}, as it is geometrically favored. This trend holds for each

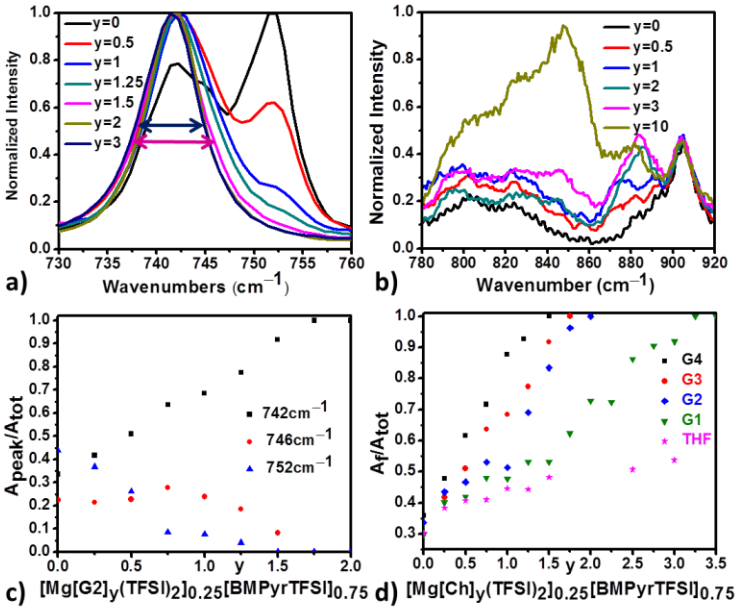

Figure 14: a) 730cm^{-1} to 760cm^{-1} Raman shift spectral region. Spectra compare vibrational excitations from additions of G3 to an initial $[Mg(TFSI)_2]_{0.25}[BMPyrTFSI]_{0.75}$ composition. b) Region of the spectra in which ether oxygen vibrational modes are prevalent. c) Fractional areas under the three fit peaks. d) Fraction of $TFSI^-$ that are free vs. added chelator.

This led us to work with pegylated ionic liquids. In these materials the cation of the IL has a polyether, or PEG, chain attached in place of one of the alkyl chains. This is essentially like having the glymes attached to the cation. It is not obvious that such an arrangement would preferentially coordinate Mg2+, as the positive charge from the IL cation might interfere. What we found is that the PEGs, attached to the IL cation do, in fact, coordinate Mg^{2+}. What this means is that Mg^{2+} is now solvated by the IL cations, rather than the anions, or a neutral chelating agent. Figure 15 shows the effect of using 1,2-dimethyldiethyleneglycolimidazolium (MMPEG2Im), MMPEG3Im and ethylhexaethyleneglycolpyrrolidinium cations (MPEG6Pyr) with $TFSI^-$ anions ILs. Dashed lines indicate the concentration of $Mg(TFSI)_2$ at which the ether oxygen to Mg^{2+} ratio is 6/1.

Mg/Mg^{2+} Electrochemistry in BMPyrTFSI:

The story for the electrochemistry of conventional magnesium salts in BMPyrTFSI remained mostly the same. Most voltammograms that showed any signs of deposition and stripping waves were only capable of stripping no more than 1mC/cm^2 of charge, meaning only 1-3 monolayers of Mg were being plated. This was found to be the case no matter how long the potential was held in this deposition region and even these results could be difficult to reproduce. Increasing the temperature did reduce the overpotential associated with electrodissolution of the deposited layer but did not change the fact that only a few layers of Mg could be removed (see figure 16). In the

previous reporting period we speculated that this could be an underpotential deposition (UPD) phenomenon; especially because these waves appeared to be approximately 1V positive of where bulk Mg deposition was assumed to be happening. At the time we were using quasi references, platinum wire and magnesium ribbon. Magnesium ribbon does not provide a true reference in these solutions because the Mg/Mg^{2+} couple is not reversible. Thus, the precise potentials at which the processes were occurring was not entirely clear. However, we were able to use Mg ribbon immersed in a 1M EtMgBr/THF solution as a true Mg reference. The solution was separated from the $Mg(TFSI)_2$/BMPyrTFSI solution by putting it in a Pasteur pipette sealed around a piece of Pt wire. This essentially acted the same as fritted glass in many well-known aqueous reference electrodes. What we found when using the true Mg reference was that the cathodic current associated with deposition of a few monolayers occurs right at 0V vs. Mg and that the anodic current associated with stripping of the Mg occurs at about 1V vs. Mg. Thus, we concluded that these processes are not Mg UPD but are in fact Mg deposition at its thermodynamic potential and dissolution at a required overpotential. As seen in figure 17, bulk Mg electrodeposition required about 1V of overpotential and could be electrochemically removed with about 20% coulombic efficiency at 100°C under dynamic vacuum conditions. This was also difficult to reproduce and could only be done under such extremely inert conditions. This was explained through an understanding of the unique nature ionic liquids. Because they are composed solely of ions, the double layer of ionic liquids must consist of packed ions of opposite charge to that of the electrode. It is likely the case that this packed layer hinders the ability for Mg^{2+} to access the electrode and

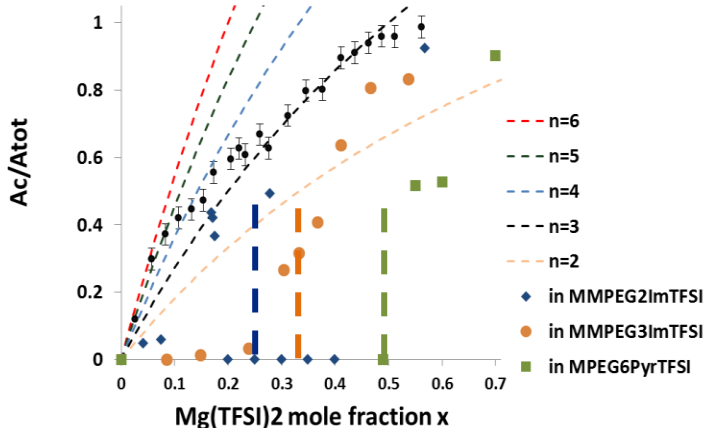

Figure 15: Mg(TFSI)2 dissolved in Pegylated ionic liquids with varying numbers of ether oxygens in the PEG chain attached to the cations. The number of ether oxygens is indicated by n in PEGn (given in the molecular acronyms).

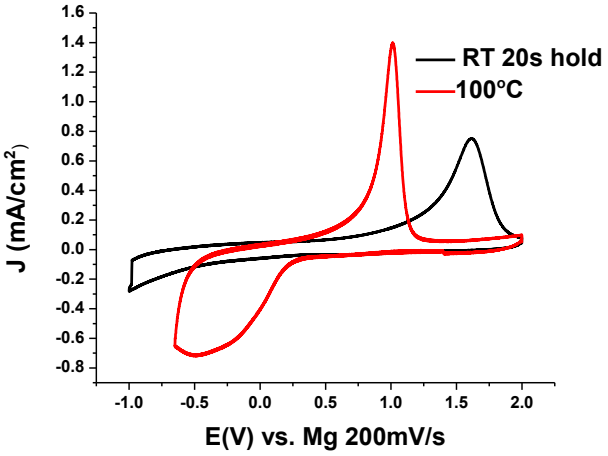

Figure 16: Comparison of 100mM $Mg(TFSI)_2$ in BMPyrTFSI at a 100C and room temperature (RT). The RT scan was paused at -0.95V vs. Mg for 20s which led to a higher anodic peak than no hold.

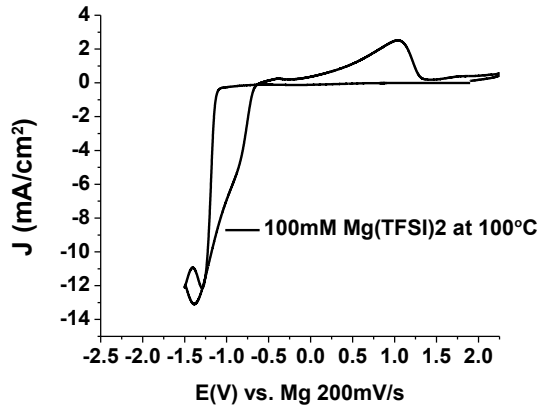

Figure 17: Cyclic voltammogram showing low coulombic efficiency electrodissolution of Mg^{2+} from a bulk Mg deposition at 100°C and dynamic vacuum.

thus only a very small amount of Mg^{2+} is able to be reduced at the thermodynamic Mg reduction potential. On the reverse sweep, Mg is unable to oxidize until the working electrode is back to around the open circuit voltage and the packed layer has dispersed, allowing Mg^{2+} into the solution. Furthermore, the solvation mentioned above, in which Mg2+ is solvated by 3 or more TFSI– is also unfavorable for migration of Mg2+ toward the negative electrode, thus adding to the kinetic barrier for bulk Mg reduction. Finally, several groups have mentioned the instability of the TFSI– anion at negative potentials, potentials near 0V vs. Mg, a phenomenon we have also observed. The voltammogram in figure 16 shows that BMPyrTFSI begins showing cathodic current near 0V vs. Mg, nearly 1V positive to the cathodic current associated with BMPyr+ reduction. This is an intrinsic property of the IL and is almost certainly TFSI– reductive decomposition. This decomposition process leads to products that inevitably create insoluble Mg salts at the electrodes surface.

New PEGylated ILs

All of these results described above led us to design and synthesize a new set of ionic liquids bearing polyethylene glycol chains as pendent groups. Thus, during 2015 and 2016 we explored the use of PEGylated ILs (see figure 18) with the idea that they may be used to create the complex conditions needed to create electrochemically active Mg species. The nomenclature used for the discussion of the PEG-ILs is written as $MPEG_mPyrTFSI$ (M = methyl group, PEG = methyl terminated polyethylene glycol chain, m = number of ether oxygens in PEG chain, Pyr = pyrrolidinium and TFSI is the bis(trifluorosulfonyl)imide anion). Our first "proof of concept" came from the use of $Mg(BH_4)_2$ as a Mg salt source. $Mg(BH_4)_2$ had been shown to provide reversible deposition/dissolution of Mg in the literature when dissolved in ethereal solvents. $Mg(BH_4)_2$ is particularly interesting because it does not corrode common electrode and battery casing materials the way many other promising Mg electrolytes do. $Mg(BH_4)_2$ was also the first example of an all inorganic Mg salt to show reversible deposition/dissolution of Mg. During this period we reported the first findings of indisputable reversible Mg deposition/dissolution from a purely ionic liquid solution using $Mg(BH_4)_2$/PEG-ILs.

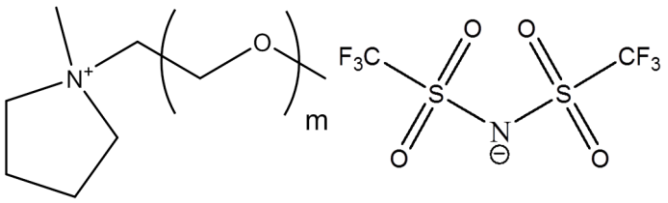

Figure 18: General molecular structure for PEGylated ionic liquids used in this study.

Electrochemical Performance of Mg^{2+} in PEG ILs:

Cyclic voltammetry (CV) was used to assess the electrochemical and chemical reversibility of Mg deposition/dissolution from $Mg(BH_4)_2$/PEG-ILs. Figure 19 compares results from $Mg(BH_4)_2$ in BMPyrTFSI, $MPEG_3PyrTFSI$ and $MPEG_7PyrTFSI$. It is clear from the CVs that $Mg(BH_4)_2$ in the non-PEG-IL (BMPyrTFSI) showed a lack of reversibility while the PEG-IL systems were able to maintain deposition and dissolution currents for successive cycles. The potentials at which the currents are observed and the general nature of the voltammograms is highly suggestive of metal deposition and stripping on the electrode surface. More detailed evidence for the nature of the Mg deposit is given in figure 20. An XRD spectrum, SEM images and EDS spectrum all indicate a smooth, dendrite free, Mg deposit was formed on a gold electrode.

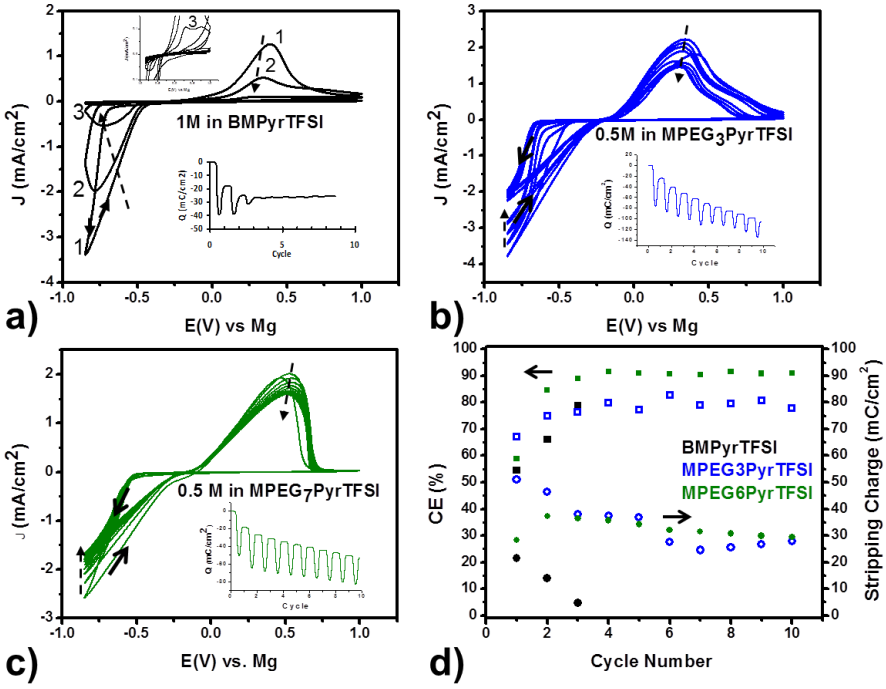

Figure 19: Successive cyclic voltammograms for a) 1M $Mg(BH_4)_2$/BMPyrTFSI, b) 0.5M $Mg(BH_4)_2$/$MPEG_3PyrTFSI$, c) 0.5M $Mg(BH_4)_2$/$MPEG_7PyrTFSI$. d) Coulombic efficiencies (CE) (squares) and stripping charges (circles) for each cycle are given. Data for the BMPyrTFSI electrolyte is presented as solid black data points. Data for the $MPEG_3PyrTFSI$ is presented as open blue data points. Data for the $MPEG_7PyrTFSI$ electrolyte is presented as solid green data points. All CVs were run in a 3 electrode cell at 25 mV/s (3 mm Pt disk working and Mg ribbon counter and reference electrodes).

Along with allowing reversible deposition and dissolution at the anode there is evidence that the PEG-IL systems are compatible with intercalation cathodes as well. Figure 21 shows Mg insertion (cathodic peak) and de-insertion (anodic peak) from the chevrel phase cathode Mo_6S_8. This significant finding revealed that the PEG-IL strategy should be generally applicable to Mg battery formulations.

Mg Speciation:

Turning to Raman spectroscopy we identified the chelating role played by the PEG chains. Raman spectra in the region of the most intense, and coordination sensitive, $TFSI^-$ peak are shown in figure 22. It is observed that for $Mg(BH_4)_2$/BMPyrTFSI solutions a Mg-TFSI peak increases in relative intensity with respect to a free $TFSI^-$ peak as the concentration of $Mg(BH_4)_2$ increases. This indicates that $TFSI^-$ anions solvate—or create complexes with—the Mg^{2+} ion in solution. The average number of $TFSI^-$ coordinating a given Mg^{2+} ion is quantified by

integrating under the peaks of modeled fits to the spectra. The fraction of $TFSI^-$ that are coordinating Mg^{2+} in the solution (A_c/A_{tot}), as a function of $Mg(BH_4)_2$ concentration, is given in figure 22b. $Mg(BH_4)_2$ averages only one $TFSI^-$ in the Mg^{2+} first solvation shell, as opposed to $Mg(ClO_4)_2$ which averages two $TFSI^-$ in analogous solutions. This shows that BH_4^- is a stronger coordinating anion than is ClO_4^-, and suggests that the likely Mg complex in solutions of all concentrations studied is the anionic $[Mg(BH_4)_2TFSI]^-$.

The idea behind the chelating ILs was to remove $TFSI^-$ from the Mg^{2+} solvation shell without the use of any neutral additives, thus maintaining a purely ionic solution. The green dashed curve of figure 22a is from an electrolyte with composition $[Mg(BH_4)_2]_{0.35}[MPEG_7PyrTFSI]_{0.65}$. Clearly, there is no sign of coordinated $TFSI^-$ in the spectrum, despite the significant concentration of Mg. In the 800–900 cm^{-1} region (not shown here) a C-O-C (from the PEG chain) stretching peak indicating Mg-O coordination is observed.

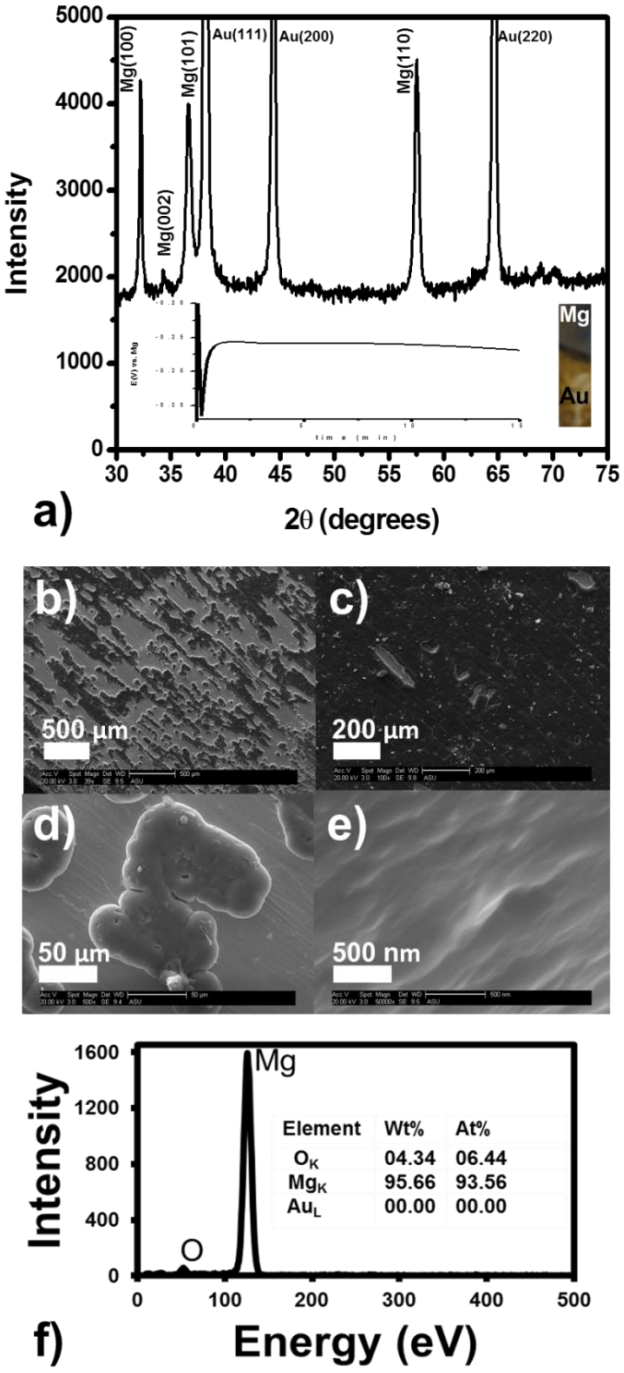

Figure 20:a) XRD pattern showing Mg deposit and Au substrate peaks. Below the XRD pattern (to the left) is a chronopotentiogram from the first 15 minutes of the 0.1 mA/cm2 deposition; to the right is an image of the Mg deposit on the Au foil substrate. b), c), d) and e) are SEM images at 39x, 100x, 500x and 50,000x respectively. f) EDS spectrum for sample portion in image (e).

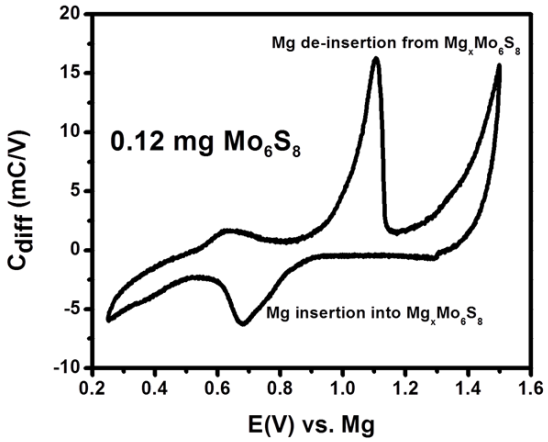

Figure 21: Slow scan rate CV at room temperature of the 2nd cycle for Mg insertion into and de-insertion from a Mo_6S_8 cathode; shown as the differential capacitance (current divided by the scan rate). The scan rate used was 100 μV/s. The electrolyte was 0.5 M $Mg(BH_4)_2$/MPEG$_7$PyrTFSI.

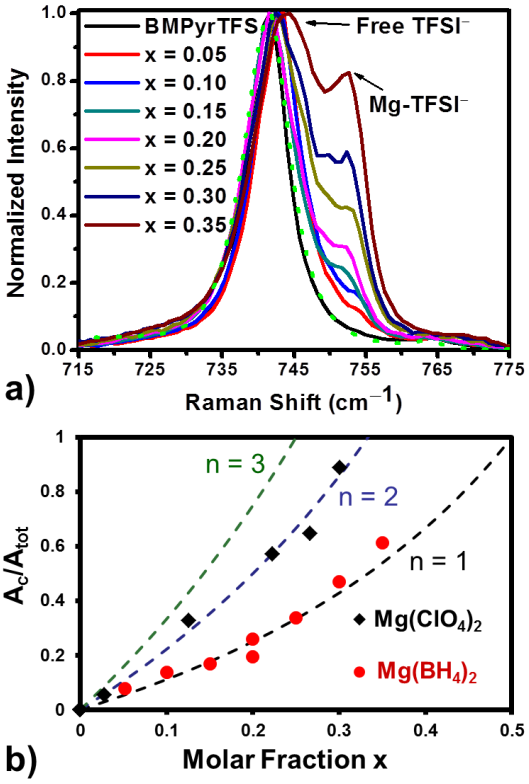

Figure 22: a) Raman spectra (715–775 cm^{-1}) for $[Mg(BH_4)_2]_x[BMPyrTFSI]_{1-x}$ electrolytes. The dashed green curve observed overlapping the black spectrum is for $[Mg(BH_4)_2]_{0.35}[MPEG_7PyrTFSI]_{0.65}$. b) Fraction of $TFSI^-$ in coordination with Mg^{2+} (A_c/A_{tot}) as a function of the molar fraction (x) of $Mg(BH_4)_2$. Dashed lines represent the theoretical trends for the average number of $TFSI^-$ coordinating Mg^{2+} (n) for n = 1, 2 and 3.

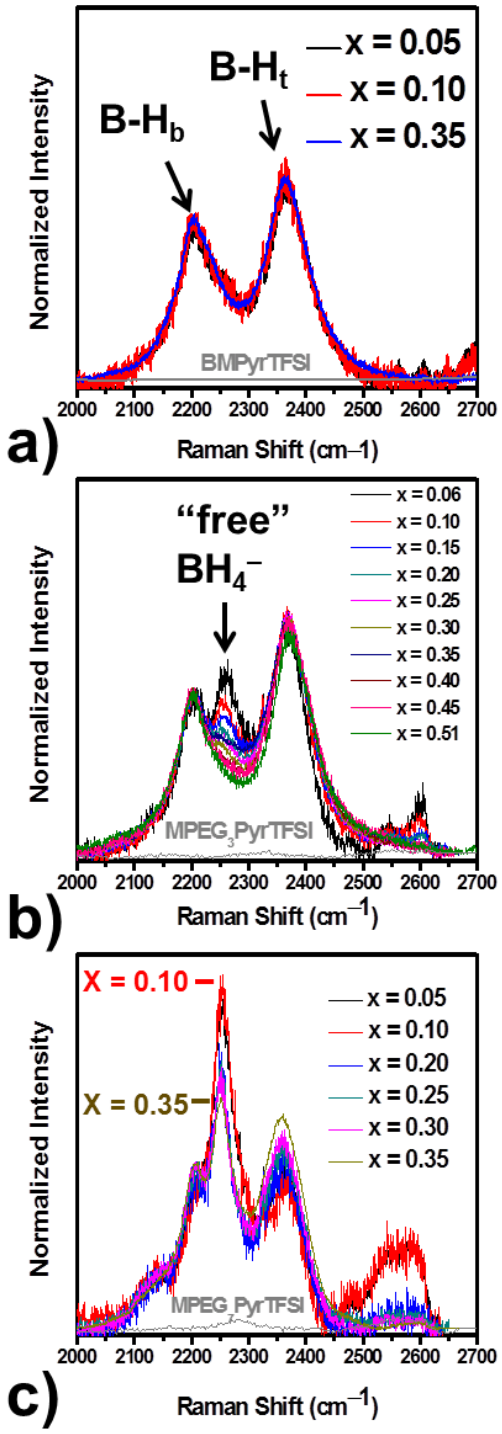

Figure 23: Raman spectra in the B-H stretching region at given molar fractions of $Mg(BH_4)_2$ (x) for a) BMPyrTFSI, b) $MPEG_3PyrTFSI$ and c) $MPEG_7PyrTFSI$. Gray curves, without any peaks, in each figure are the spectra of the respective pure IL.

Figure 23 shows the B-H stretching region. In figure 23a a range of $Mg(BH_4)_2$ concentrations in BMPyrTFSI are displayed. No change is observed as the concentration of the Mg salt is increased. In the literature, several researchers have assigned the higher and lower frequency B-H peaks to terminal and bridging hydrogens, respectively—of coordinated BH_4^-. On the other hand, in figure 23b a separate peak is observed in the $Mg(BH_4)_2$/$MPEG_3$PyrTFSI system and assigned to freely dissociated BH_4^- (indicated in the figure). The peak is stronger at lower $Mg(BH_4)_2$ concentrations. The free BH_4^- peak is found to be even stronger in the PEG_7-IL system, shown in figure 23c. The dependence on concentration is still not fully understood. To increase our confidence in the free BH_4^- assignment we acquired Raman spectra of solid tetrabutylammoniumborohydride (Bu_4NBH_4) and a 1 M solution of Bu_4NBH_4/BMPyrTFSI. Figure 24 compares the Bu_4NBH_4 samples with the lowest concentration of $Mg(BH_4)_2$ observed in $MPEG_7$PyrTFSI. The B-H stretching peek in 1 M Bu_4NBH_4/BMPyrTFSI must correspond to freely dissociated BH_4^- as Bu_4N^+ is a very weakly coordinating cation. We thus feel safe with the free BH_4^- assignment. The significance of the Raman results is that higher order PEG chains lead to a greater degree of BH_4^- dissociation. We are currently looking into quantifying the various Mg-BH_4 complexes and determining what role the complexes play in the reversible electrochemistry. While identification of the free BH_4^- is interesting, its role in the reversible deposition/dissolution process is not yet clear. It could be that a greater concentration of free BH_4^- enhances the Mg dissolution kinetics but this is still rather speculative. However, what appears to be most important is that TFSI– is removed from the first solvation shell of Mg^{2+}. The results suggested that $Mg(BH_4)^+$ may be the complex undergoing the first reduction, likely followed by desorption of BH_4^- and the very fast subsequent, or simultaneous, reduction of Mg(I). This is certainly plausible considering BH_4^-'s superior reductive stability with respect to $TFSI^-$. This very strongly suggested that in order to achieve reversible Mg deposition and dissolution, one needed the presence of "free" (i.e. not coordinated) borohydride. Thus, we turned to a simpler experimental system in which we could independently vary the concentration of BH_4^- and glyme coordinating ligands.

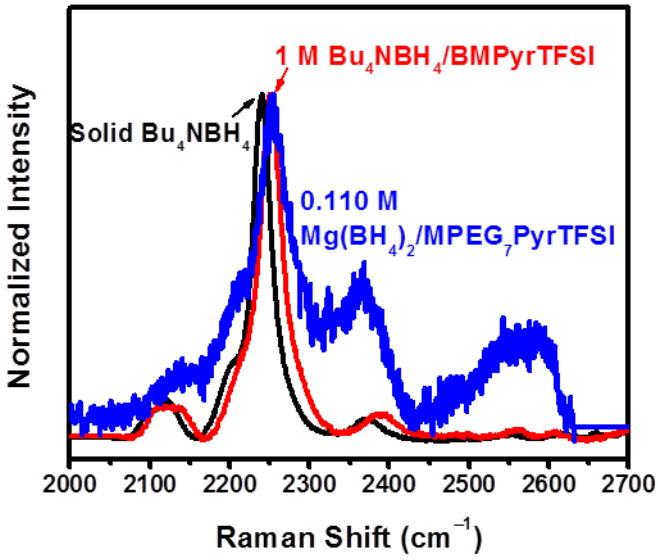

Figure 24: Raman spectra in the B-H stretching region for solid Bu_4NBH_4 (black), 1 M Bu_4NBH_4/BMPyrTFSI (red) and 0.110 M $Mg(BH_4)_2$/$MPEG_7$PyrTFSI (blue).

Electrochemistry of Mg^{2+} in "normal" BMPTFSI with added BH_4^- and glymes

Our final effort explored whether we could replicate the behavior we observed in the synthetic PEG-modified ILs simply by addition of BH_4^- (to control water content) and glymes (to prevent Mg^{2+} speciation as $Mg(TFSI)_3^-$ and to prevent reductive fragmentation of $TFSI^-$ that obviously led to electrode fouling.

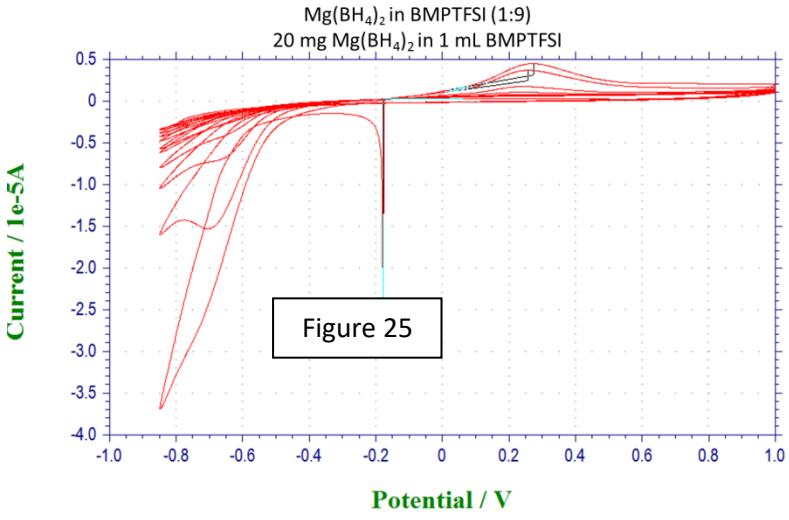

Our past work had shown that the influence of Mg^{2+} chelation by polyether chains can dramatically influence the reversibility of Mg electrodeposition. Also, the presence of BH_4^- has been shown to be beneficial. In this final reporting period we explored the impacts of adding both BH_4^- and glyme together.

Borohydride additions

We did a number of experiments in which BH_4^- was added to various electrolytes to explore the extent to which water scavenging can have beneficial effects on Mg electrodeposition. Figures 25 and 26 show examples of this effect. Figure 25 shows repetitive CVs of Mg electrodeposition in BMP TFSI. The Mg^{2+} salt is $Mg(BH_4)_2$. Figure 26 shows the corresponding plot of charge versus time for the CV in Figure 1. As can be seen, even though BH_4^- is present, reversibility if limited. This is both because the BH_4^- is coordinated to Mg^{2+}, making it less reactive toward water, and because the Mg^{2+} center is still available for interactions with $TFSI^-$. As we described in our last publication, the Mg^+ intermediate formed during Mg electrodeposition reductively fragments $TFSI^-$, causing electrode fouling. Thus, these conditions are not suitable for reversible Mg electrodeposition.

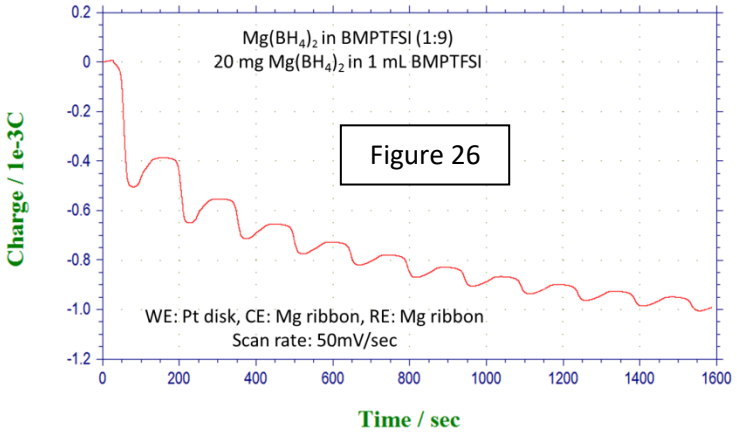

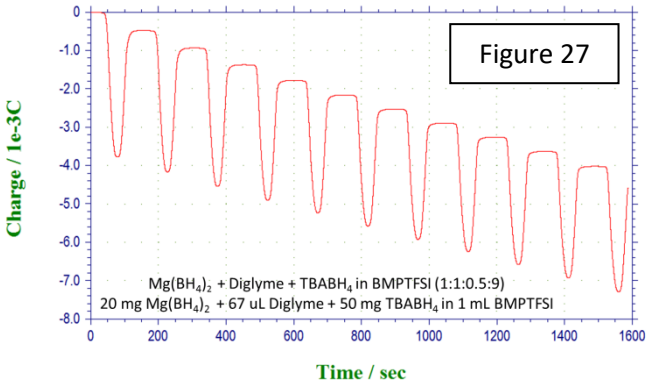

In contrast, if we add both a glyme solvent and free BH_4^- (by adding tetrabutyl ammonium borohydride, $TBABH_4$), the reversibility is dramatically improved. Figure 27 shows an example of this. Here by simple addition of a chelation agent and "free" BH_4^-, we achieve fairly reversible Mg electrodeposition with coulombic efficiency near 90%. Note that diglyme is the chelator added in this case. We expect superior results with longer glyme chains.

Final results and assessment:

The project demonstrated that it is possible to achieve reversible electrodeposition and dissolution of Mg^{2+}/Mg using a PEG chain complexation approach that mitigates three separate issues for the Mg system. The first issue is speciation of Mg^{2+}. In TFSI electrolytes, Mg^{2+} is speciated as $Mg(TFSI)_3^-$. This anionic form of Mg^{2+} causes the electromigration of Mg^{2+} to be counter to the direction needed for efficient electrodeposition. Coordination with PEG chains displaces the $TFSI^-$ and prevents this situation. Second, displacement of $TFSI^-$ from the inner coordination sphere of Mg^{2+} by PEG chain coordination also suppresses $TFSI^-$ fragmentation caused by reaction with the Mg^+ redox intermediate that is part of the Mg^{2+}/Mg redox couple. This fragmentation causes fouling of the electrode surface and prevents good cycling. Again, coordination with PEG chains prevents this situation. Third, use of electrolytes containing BH_4^-, especially free BH_4^-, causes scavenging of free water, which prevents electrode fouling by reaction of trace water with the Mg metal after deposition. So, the combination of PEG chain coordination and use of electrolytes containing BH_4^- proved to be a potent combination that enabled reversibility of the Mg^{2+}/Mg redox couple with current densities and Coulombic efficiencies that were that best that had been observed in ionic liquid media at the time. The results of this effort are described in full detail in the manuscripts and supporting materials reported as part of this final report and the interim reports submitted during the project.

Outcomes during This Project Period:

Patents:

An invention disclosure was submitted to the Arizona State University technology transfer office (Skysong Innovations) entitled: *Chelating Ionic Liquids for Magnesium Battery Electrolytes*. The office filed a provisional patent application, which was subsequently converted to a full patent application. That application was just published, as United States Patent Application 20180233781, CHELATING IONIC LIQUIDS FOR MAGNESIUM BATTERY ELECTROLYTES AND SYSTEMS.

Manuscripts:

Pubilished papers are given in the other sections of the final report. In addition, a manuscript on the addition of glymes and BH_4^- to Mg^{2+}-containing solutions is being prepared. This paper will

also include some of our preliminary work on Ca^{2+}, which will be reported as part of our renewal effort at ARO.

Presentations:

A poster on the $Mg(BH_4)_2$/PEG-IL work in ILs and PEG-ILs entitled "*Designer Ionic Liquids for Improved Magnesium Anode Behavior*" was presented at the Gordon research Conference in Newry, Maine, Aug 14-19, 2016.

An invited keynote address on the $Mg(BH_4)_2$/PEG-IL work in ILs and PEG-ILs entitled "*Designer Ionic Liquids for Improved Magnesium Anode Behavior*" was given at the Fall 2016 Electrochemical Society meeting of in October in Honolulu, Hawaii.

An invited presentation on the $Mg(BH_4)_2$/PEG-IL work in ILs and PEG-ILs entitled "*Designer Ionic Liquids for Improved Magnesium Batteries*" was given at the annual workshop on electrochemistry at University of Texas, Austin, in February 2017.

An invited presentation on the $Mg(BH_4)_2$/PEG-IL work in ILs and PEG-ILs entitled "*Ionic liquids for next generation energy applications*" was given at the Gordon Research Conference on Ionic Liquids at Newry, Maine, Aug. 12-17, 2018.